Some Dynamic Mechanical Properties of Distended Carbons

L. M. Lee,* R. P. May,* and T. R. Guess†
Sandia Laboratories, Albuquerque, N. Mex.

An experimental study to define the dynamic response of seven distended carbon materials to shock loading is described and the results are presented. The study included measurement of equation of state parameters to 235 kilobars, unloading behavior, and spallation strengths. In the low-stress (partially compacted) region, the response to shock loading was found to be dependent on the initial structure of the material, i.e., form of carbon and initial density, while in the high-stress region the response was primarily affected by the initial density. The results of the unloading wave experiments, attenuation data, and higher pressure free surface velocity measurements indicated that the unloading behavior of these materials was a function of the applied pressure in the partially compacted region. Accordingly, the Hugoniot data were closely represented by a previously proposed empirical model which describes the response of partially compacted porous materials. The spallation results show differences in the dynamic tensile strengths varying from 0.4–1.0 kilobar, depending on the material.

Nomenclature

c_0 = bulk wave velocity
$\mathcal{E}$ = internal energy
P = pressure
P_s = stress to produce complete void collapse
s = slope of linear $U_s - u_p$ fit
u_{fs} = free surface velocity
u_p = particle velocity
U_s = shock velocity
v = specific volume
α = distention ratio ρ_s/ρ_F
γ = Gruneisen parameter
ρ_F = distended material density
ρ_0 = initial density
ρ_s = solid material density
σ = stress

Introduction

THE need for carbon materials in heat shield applications has resulted in the continuing development of new carbon systems. All of these systems have the common characteristic of some degree of porosity, but they differ in structure (form of carbon). Consequently, the variable porosity and structure, which are sensitive to methods of processing, result in a set of very complicated materials. Furthermore, the dynamic properties of these materials are dependent on both the degree of porosity and the structure. Before a material can be considered for use, its equation of state is required as input for design calculations. Presently, however, the dynamic properties of materials can only be determined experimentally, and often a large number of tests must be conducted on a single material to describe it adequately. Conducting an extensive experimental program on each new carbon system of interest obviously would be impractical. Therefore, a means of estimating the equation of state of porous materials with a minimum of experimental work is needed.

This paper describes a study in which seven carbon materials were subjected to uniaxial-strain shock loading. The primary objective of the study was to determine the loading equation of state behavior of all seven systems, the unloading behavior of one system, and the spallation strengths of five systems. A secondary but very important objective of the study was to find a suitable model which, when used with a minimum of experimental data, would reproduce, at least in gross detail, the experimentally observed data. In the discussion section, an attempt will be made to show the extent to which the model is able to describe the experimental loading data of the seven carbon systems considered.

Material Description

Carbon can exist in amorphous, mesomorphous, graphite, and diamond forms. Material properties of these forms vary extensively as evidenced by the density of the "pure" allotropes: 1.88 g/cc for amorphous carbon, 2.25 g/cc for crystalline graphite, and 3.51 g/cc for diamond.[1,2] The materials of this report were either highly amorphic, highly graphitic, or mesomorphic. The mesomorphic materials were predominantly amorphous and can be classed as amorphous. All were porous.

Table 1 contains significant information pertaining to fabrication of the seven materials studied where the designations C/C and PCF-CVD are clarified in the notes to the table. These materials were manufactured by either the Bendix Corp., Kansas City Division (BKC), the Union Carbide Corp., Y-12 Plant (Y-12), or by Sandia Laboratories, Albuquerque (SLA). Of the seven materials, the five C/C's were all fabricated in the same manner, but were individually characterized by varying extents of two significant properties. The final density, which is an indication of porosity, was one of these important material properties, and the final graphitization state was the other. Fabrication of a C/C begins with layers of amorphous carbon or graphite cloth impregnated per Table 1. This impregnated cloth layup is cured at pressures of approximately 500 psi at temperatures near 160°C for 12–24 hours. Curing is followed by a carbonization cycle in an inert atmosphere. The BKC materials were carbonized, reimpregnated, and recarbonized for a total of four carbonizing cycles, each cycle exceeding 120 hours (5 days) and reaching a maximum temperature of 840°C. The Y-12 material, C/C-0, went through three carbonizing and reimpregnation cycles each of ten days duration at temperatures up to

Presented at the ASME/AIAA 10th Structures, Structural Dynamics and Materials Conference, New Orleans, La., April 14–16, 1969 (no paper number; published in bound volume of conference papers); submitted April 21, 1969; revision received February 2, 1970. This research was supported by the U.S. Atomic Energy Commission. The authors thank S. F. Duliere of Sandia Laboratories, Division 5522, for the X-ray powder diffraction analysis. Sandia personnel at the Division 5161 air gun facility and Division 5163 firing site contributed greatly in preparation of experimental assemblies and performance of experiments.

* Solid Dynamics Research Department.
† Composites Research and Development Department.

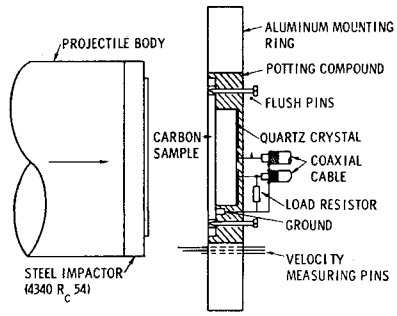

Fig. 1 Configuration for transmitted wave experiment.

1000°C with the final cycle taken to 1400°C. The C/C-4 was processed identically to C/C-1 except that it was staked with carbon filaments normal to the plane of the cloth in an attempt to improve the delamination properties. The stakes were 0.010-in.-diam filaments with a center-to-center spacing of 0.050 in.

The two PCF materials began with carbonized rayon felts which were heated to 1100°C and infiltrated with methane gas.[3] Decomposition of the methane on the hot felt produced the deposited carbon matrix. The graphitized material, PCF-CVD-G, was subjected to a further heat treatment of two hours at 3070°C.

The type of carbon in each material was identified by powder diffraction using monochromatic x-rays and a Debye Scherrer camera. The x-ray diffraction patterns of graphite and amorphous carbons are distinctive; a value of interplanar spacing for graphite of 3.35 Å and a diffuse pattern for amorphous carbon centered around 3.44 Å are generally accepted.[1] Three materials (C/C-2, C/C-3, PCF-CVD-U) showed the diffuse first diffraction ring associated with amorphous carbon. This ring spacing is listed in Table 2. The C/C-0 and PCF-CVD-G showed the clear crystalline pattern of graphite with some diffuseness of the diffraction lines. This line broadening gives an indication of particle size in the c crystallographic direction. Crystallite sizes calculated from the line broadening are listed in Table 2. The remaining two materials, C/C-1 and C/C-4, show both the graphite and amorphous carbon spacing. The graphite crystallite sizes for these two mesomorphs are given in Table 2. The size of the amorphous particles are not listed but are less than 25 Å.

From the preceding description, conclusions can be drawn concerning each material. Density is a fair measure of distention. Temperature-time histories, x-ray diffraction, and form of carbon used in fabrication give a good indication of the degree of graphitization. These factors indicate that C/C-2, C/C-3, and PCF-CVD-U are porous, amorphous carbon. C/C-0, C/C-1, C/C-4, and PCF-CVD-G are all graphitic to varying degrees. C/C-1 and C/C-4 initially contained 11% of graphite powder and were never exposed to temperatures above 840°C so it is reasonable to assume a total graphite content of 11–15%. Based on this, C/C-1 and C/C-4 were classed as amorphic. The C/C-0 and PCF-CVD-G are predominantly graphite as would be expected from the initial use of graphite and from the processing temperature of 1400°C for C/C-0 and 3070°C for PCF-CVD-G.

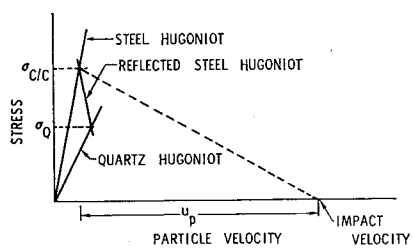

Fig. 2 Impedance match solution for buffer plate experiment.

Experimental Techniques and Data Analysis

The dynamic response of the carbons was studied under conditions of uniaxial-strain shock loading. The stress pulse was produced in the carbon specimens either by using a gas gun to impact a flat plate with the specimen or by explosive loading. All experimental measurements were made while the specimen was in a uniaxial-strain condition. By varying the experimental configuration and instrumentation, the compressive loading, unloading, and spall strength data were experimentally determined. In addition, attenuation experiments were made at the Boeing Company by using an exploding foil to fly a thin plate against the specimen. The results of these attenuation experiments are included in this report. For the data analysis, it was assumed that the stress pulse propagated as a steady wave with thermodynamic equilibrium behind the shock front and that the Rankine-Hugoniot jump equations were applicable.

Compressive Loading Data

Air gun experiments

The low-stress experimental data defining the loading Hugoniot characteristics below 40 kbars were obtained from three types of plate-impact experiments performed with a gas gun.[4] The first experimental configuration, shown in Fig. 1, is referred to as a transmitted wave experiment since it is designed to measure the stress profile after it has propagated through the carbon sample. In this configuration, a 4340 steel (R_c 54) projectile nose was impacted against the carbon sample.[5] The stress pulse generated by the impact propagated through the sample and interacted with an x-cut quartz crystal mounted on the rear surface of the sample.[6] The parameters measured included the impact velocity, tilt, and current output of the quartz gage across a 50 ohm termination resistor. The time of impact and tilt were obtained from flush pin records.[4] The quartz was used to detect the structure of the transmitted stress wave, and in conjunction with the flush pin records, to measure transit time of the stress wave through the carbon sample.[6] Two types of wave structures were detected. For the two graphitic carbons, the wave profile was a single jump in stress. However, the amorphic carbon systems supported a ramp-shaped precursor propagating ahead of the main stress wave. The data reduction technique used for the transmitted wave experiments was an impedance match solution.[7]

Table 1 Material identification

Specific designation	Nominal density, g/cc	Manufacturer	Substrate	Impregnation blend
C/C-0[a]	1.51	Y-12	Graphite cloth	Graphite powder, carbon black, furfuryl alcohol, acetone
C/C-1	1.40	BKC	Amorphous cloth, Pluton H25-15 end roving	Epoxylated novolac resin, 11% graphite powder
C/C-2	1.38	BKC	Amorphous cloth, Pluton H25-15 end roving	Durez resin, PR275 pitch
C/C-3	1.34	BKC	Amorphous cloth, basic CY-2-5 end yarn	Durez resin, PR275 pitch
C/C-4	1.40	BKC	Amorphous cloth, Pluton H25-15 end roving, staked	Epoxylated novolac resin, 11% graphite powder
PCF-CVD-U[b]	1.76	SLA	Amorphous felt	Methane gas
PCF-CVD-G[c]	1.71	SLA	Amorphous felt	Methane gas

[a] C/C refers to Carbon matrix/Carbon binder.
[b] PCF-CVD-U refers to pyrolytic carbon felt-carbon vapor deposited-ungraphitized.
[c] PCF-CVD-G refers to pyrolytic carbon felt-carbon vapor deposited-graphitized.

In the second plate-impact experimental configuration, designed to obtain low-stress compressive loading data, a projectile mounted carbon sample was impacted against an x-cut quartz gage. These are referred to as direct impact experiments. The projectile impact velocity and quartz gage output were monitored in the same manner as the transmitted wave experiments. The measured quartz voltage, impact velocity, and known elastic properties of the quartz are sufficient to determine a stress-particle velocity (σ, u_p) data point for the carbon.[7] This experiment, however, does not define the actual path followed by the carbon in loading to an equilibrium state at the (σ, u_p) data point. There must be some knowledge of the loading path prior to calculation of the shock velocity, U_s, and specific volume, v, associated with the (σ, u_p) data point. The loading path of the material is obtained from the transmitted wave experiments. For those materials without precursors, the parameters U_s and v were calculated directly using the Hugoniot jump equations. For those carbons supporting a precursor, an elastic-linearly plastic loading assumption was used in conjunction with the precursor state point, as calculated in the transmitted wave experiments, to determine the appropriate U_s and v parameters associated with the final state point of the carbon.

In the third experimental configuration, which is referred to as a buffer plate experiment, a projectile mounted carbon sample was impacted against a 4340 steel (R_c 54) buffer plate backed by a quartz gage. The high-impedance buffer plate was used to obtain higher stress levels than those obtained by impacting the quartz directly. The projectile impact velocity and quartz gage output were monitored as previously described. A schematic illustration of the method of solution used to reduce the buffer plate experiments is shown in Fig. 2. Impedance match calculations at the buffer-quartz interface yield the elastic σ, u_p condition in the buffer prior to the stress wave interaction at that interface. The boundary conditions of continuity of stress and particle velocity across the carbon-buffer interface at impact were used to calculate the maximum stress and total change in particle velocity for the carbon sample, i.e., its final (σ, u_p) data point. The same arguments can be made in this experiment as in the direct impact experiments concerning the calculation of the shock velocity and specific volume associated with the (σ, u_p) data point. For those carbons to which it applied, the effect of the precursor was considered in the calculations.

High-explosive experiments

The loading or compressive Hugoniot data of the carbon systems at stresses above 40 kbars were obtained by standard explosive techniques. Two types of experimental setups were used. In the first configuration (Fig. 3), a carbon specimen and a standard material specimen were placed on a standard material driver plate that was in direct contact with various explosive assemblies. The materials used for standards were 4340 steel, copper, plexiglas, or 2024 aluminum, all of which have documented equations of state.[5,8,9] The

Table 2 Results of x-ray powder diffraction

Material	Spacing, Å: Graphitic (002)	Spacing, Å: Amorphic interlayer	Crystallite size, Å	Remarks
C/C-0	3.41	...	150	Predominately graphite
C/C-1	3.37	3.70	183	11–15% graphite
C/C-2	...	3.75	<25	No graphite
C/C-3	...	3.50	<25	No graphite
C/C-4	3.37	3.70	250	11–15% graphite
PCF-CVD-U	...	3.45	60	No graphite
PCF-CVD-G	3.36	...	235	Predominately graphite

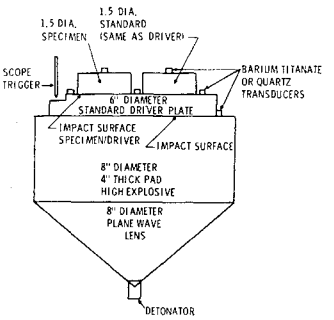

Fig. 3 Explosive-specimen assembly for impedance match tests.

stress to which the carbon was shock loaded was dependent on the choice of standard material and explosive. Instrumentation consisted of an x-cut quartz gage mounted on the back surface of the carbon sample to monitor the precursor (if any) in the sample and to determine arrival times of the second shock through the carbon sample. Also lead zirconate-titanate (PZT) transducers were used to determine transit times through the standard driver plate and standard specimen.

In the second configuration, two changes were made to the assembly shown in Fig. 3. First, the specimen of standard material was omitted, and second, the carbon sample size was increased to provide space for a slanted wire resistor and quartz gage. The slanted resistor is a technique for monitoring free surface motion from which free surface velocity-time (u_{fs},t) histories for the carbon samples were derived.[4]

Since all the carbons studied were initially distended, and since (within the resolution of the slanted resistor data) free surface measurements show a one-wave plastic shock structure, the final Hugoniot data were obtained using the methods of impedance matching described by Rice et al.[8]

In those experiments where free surface velocities were determined, the values are reported for comparison with the impedance match solution of the particle velocity. For solids the particle velocity should be about equal to one-half the free surface velocity; however, for these distended carbons the particle velocity was always greater than one-half the free surface velocity, the ratio being in the 0.55 and 0.66 range. This type of result has been found previously.[10]

The compressive loading Hugoniot data as determined from both the air gun and high-explosive techniques are listed in Table 3.

Unloading Wave Data

The unloading wave experiments were conducted with a gas gun. A carbon sample, having a free rear surface, was impacted against a thick lucite witness plate. At impact compressive stress waves propagated into the carbon sample and lucite plate. Upon reaching the carbon free surface, the compressive stress was reflected as a rarefaction or unloading wave that propagated back through the carbon into the lucite. The particle motion of a thin mirror embedded in the lucite was monitored as a function of time using the velocity interferometer technique developed by Barker.[11] The particle velocity-time history of the lucite as measured in this experimental configuration was dependent on the loading and unloading characteristics of both the carbon and the lucite. Since these characteristics are known for the lucite and the loading characteristics are known for the carbon (from experiments described previously), the data can be reduced to determine the carbon unloading characteristics.[12] The details of the velocity interferometer technique and data reduction techniques have been reported and are not included in this paper.[11] The results of the unloading wave experiments will be presented and discussed in a later section of this paper.

Table 3 Hugoniot data

Type of experiment	Initial density ρ_0, g/cc	Stress σ, kilobar	Particle velocity u_p, mm/μsec	Shock velocity U_s, mm/μsec	Specific volume v, cc/g	Free surface velocity u_{fs} mm/μsec
		a. C/C-0 (graphitic)				
6	1.50	3.1	0.10	2.00	0.628	
3	1.51	4.1	0.149	1.85	0.611	
1	1.48	11.9	0.353	2.26	0.569	
1	1.48	16.5	0.495	2.25	0.527	
3	1.49	21.9	0.591	2.48	0.510	
3	1.50	36.5	0.90	2.70	0.441	1.40
4	1.50	115.0	1.73	4.32	0.397	
4	1.50	173.5	2.20	5.12	0.377	
4	1.50	205.8	2.45	5.46	0.365	
		b. PCF-CVD-G (graphitic)				
2	1.69	1.3	0.070	0.84	0.542	
3	1.73	3-0	0.138	1.33	0.518	
3	1.72	8.9	0.333	1.55	0.456	
1	1.73	11.1	0.355	1.80	0.464	
1	1.72	14.7	0.431	1.99	0.455	
3	1.68	16.9	0.489	1.77	0.431	
3	1.70	21.9	0.546	2.35	0.451	
4	1.73	47.3	0.90	3.04	0.407	
4	1.73	234.9	2.38	5.71	0.338	
		c. C/C-1 (amorphous)				
1[a]	1.39	1.6	0.040	2.86	0.703	
				2.99[b]		
3	1.40	4.7	0.111	3.04	0.687	
2	1.40	5.0	0.124	2.82	0.683	
1[c]	1.36	7.6	0.228	2.30	0.667	
1[c]	1.40	7.8	0.226	2.35	0.648	
3	1.40	8.6	0.231	2.59	0.652	
2	1.40	8.9	0.248	2.48	0.644	
1[c]	1.37	12.0	0.347	2.45	0.631	
1[c]	1.41	12.2	0.326	2.59	0.622	
2	1.40	13.5	0.376	2.49	0.609	
3	1.39	15.8	0.446	2.48	0.592	
2	1.38	16.6	0.469	2.49	0.590	
3	1.36	19.8	0.509	2.77	0.592	
3	1.38	23.0	0.593	2.76	0.570	
3	1.40	25.0	0.623	2.82	0.558	
4	1.40	50.5	1.08	3.34	0.484	
4	1.40	81.1	1.51	3.83	0.433	
4	1.40	110.8	1.82	4.35	0.415	
		d. C/C-2 (amorphous)				
4,5,6[d]	1.38	1.0	0.020	3.68	0.721	
5[c]	1.38	40.8	0.85	3.47	0.548	1.53
4[c]	1.38	41.8	0.88	3.44	0.540	
4	1.38	106.1	1.77	4.34	0.429	
4	1.38	153.8	2.30	4.86	0.382	
4	1.38	181.7	2.56	5.15	0.361	
		e. C/C-3 (amorphous)				
1,5,6[a]	1.35	1.6	0.035	3.35	0.733	
				3.58[b]		
2	1.35	2.7	0.058	3.56	0.729	
2	1.35	5.5	0.123	3.17	0.711	
3	1.34	8.8	0.210	3.01	0.695	
1[c]	1.35	10.8	0.261	3.00	0.678	
2	1.36	13.1	0.299	3.17	0.670	
1[c]	1.35	17.4	0.418	3.03	0.642	
2	1.35	17.4	0.420	2.99	0.637	
3	1.34	21.6	0.510	3.11	0.627	
5[c]	1.34	42.9	0.98	3.18	0.516	1.62
5	1.34	97.2	1.73	4.17	0.436	2.87
5	1.34	144.4	2.21	4.83	0.404	3.42
5	1.34	175.6	2.50	5.20	0.386	3.76
		f. C/C-4 (staked amorphous)				
4[e]	1.40			3.58		
3	1.39	5.8	0.168	2.31	0.670	
3	1.39	12.6	0.341	2.57	0.626	
3	1.38	21.1	0.541	2.74	0.584	
4[c]	1.40	40.3	0.85	3.36	0.534	
4	1.40	65.2	1.25	3.75	0.476	
4	1.40	157.9	2.28	4.92	0.383	
4	1.40	187.9	2.52	5.27	0.373	
		g. PCF-CVD-U (amorphous)				
1[a]	1.75	1.7	0.040	2.43	0.562	
				2.70[b]		
2	1.78	2.5	0.065	1.88	0.545	
2	1.77	3.3	0.095	1.56	0.536	
2	1.79	4.2	0.116	1.82	0.526	
2	1.77	6.4	0.186	1.80	0.512	
1[c]	1.74	9.1	0.270	1.83	0.494	
2	1.78	9.6	0.248	2.11	0.497	
3	1.75	10.2	0.269	2.11	0.501	
2	1.76	11.7	0.307	2.09	0.487	
1[c]	1.75	13.3	0.358	2.04	0.474	
3	1.76	14.4	0.398	1.98	0.451	
3	1.73	23.0	0.446	2.98	0.492	
3	1.77	23.1	0.431	3.05	0.486	
3	1.81	23.8	0.458	2.87	0.464	
3	1.75	25.0	0.557	2.53	0.448	
3	1.77	30.4	0.572	2.98	0.455	
4	1.80	55.6	0.84	3.65	0.427	
4	1.75	73.1	0.95	4.39	0.448	
4	1.81	80.1	1.04	4.26	0.418	
4	1.75	151.6	1.74	4.98	0.372	

Type of experiment
1 Transmitted wave profile shot using a quartz crystal.
2 Sample impacting a quartz crystal directly.
3 Sample impacting a 4340 steel (R_c 54) plate with a quartz crysta on the buffer plate.
4 Explosive impedance match.
5 Explosive impedance match—monitored sample free surface velocity with a slanted resistor.
6 Explosive impedance match using elastic pressure in 4340 steel (R_c54) as a driver.

[a] Average of measured precursors: average ρ_0; σ, u_p, and v at plastic wave breakaway; Us at half amplitude point of precursor ramp.
[b] Average U_s of precursors at breakaway.
[c] Experiment where precursor ramp was measured.
[d] Average of measured precursors; σ, u_p, add v at plastic wave breakaway; Us at precursor breakaway.
[e] Only measured precursor for C/C-4. Buffer experiments reduced using precursor data C/C-1.

Spallation Strengths

A series of experiments was conducted to determine the spall strengths for five of the carbon systems.[13] Historically, spallation has been defined as a complete or partial separation of a material resulting from the tension induced by the interaction of two rarefaction or unloading waves.[14] However, the spall strength of the carbons tested was defined as the lowest tensile stress that produces visible damage (generally a delamination) to a carbon target.

The gas gun was used to launch a carbon impactor against a carbon target (Fig. 4). The target was a tapered plug mounted in an aluminum annular ring. The annular ring technique is designed to 1) reduce the sample size, 2) eliminate bending of the sample, 3) facilitate sample recovery, and 4) minimize the effects of side rarefactions on the target sample. As illustrated in Fig. 4, both the carbon impactor and the target had free rear surfaces, a condition that results in the production of rarefaction waves. These waves interacted in the target to produce a tensile stress pulse. The target plugs were recovered by catching them in a cotton filled recovery can attached to the rear of the annular ring.

The impact velocity of the projectile was measured as described previously, and the damage, if any, was observed on the circumferential surfaces of the recovered targets. The usual procedure of sectioning a spall target and examining it for microscopic damage was not used for two reasons: First, the carbon systems were initially distended and these voids would not be distinguishable from minute spall damage after sectioning, and second, a significant spall surface created in the interior of the target would, for most systems, propagate to the circumference of the target plug due to the brittleness of the carbon composites.

The experimental data were reduced to determine the magnitude of the spall stress and its approximate pulse duration. For the low-stress levels produced in the spall experiments, the compaction of the carbon is negligible and the wave propagation can be approximated as elastic behavior.

Using this assumption, the carbon spall strengths were determined from impact stress calculations rather than from wave propagation calculations on the spall plane. Under these conditions the duration of the tensile stress pulse on the spall plane is approximately twice the impactor thickness divided by the stress wave velocity.

Table 4 lists the approximate impact velocity for spall, the stress pulse duration, and the spall strengths (impact stress calculations) for five of the carbon systems.

Attenuation Experiments

One of the amorphous carbon systems (C/C-1) was studied in a series of experiments designed to indicate the attenuation of a narrow stress pulse as it propagated through various thicknesses of material. The experimental work was conducted by the Boeing Company, Seattle, Wash., under Sandia Laboratories Contract 16-6715.[15] The experimental data consisted of the initial free surface velocity of the carbon as a function of material thicknesses for a constant impulsive stress loading. An exploding foil technique was used to impact thin mylar plates against stationary carbon targets of different thicknesses.[16] The measurements consisted of the impact velocity of the mylar slapper and the free surface velocity of the carbon target. The velocities were measured from the apparent motion of the image of a wire reflected from a mirrored surface on the target. A rotating mirror streak camera was used to make these measurements. These streak camera records supplied by Boeing were then reduced in this study producing the experimental data as listed in Table 5.

Discussion of Experimental Results

Shock Loading of Porous Carbons

Initially a distended material has some percentage of voids distributed throughout its volume. After low-stress-level dynamic compressions of such materials, the percentage of voids per unit volume is reduced and the material is considered to be partially compacted. Ultimately at some higher stress level (P_s), all of the voids will be effectively eliminated and the material can be considered fully compacted. The dynamic response in the partially compacted region is governed primarily by the structure of the material, and its initial distention.

Pursuing the second objective of the study, loading curves for the porous carbons were then calculated for comparison with the experimentally determined Hugoniots. The response below P_s was calculated using the $P - \alpha$ model.[17] A description of the $P - \alpha$ model is given in the Appendix. The $P - \alpha$ model offers an empirical method, requiring only a minimum amount of experimental data, to describe a constitutive equation for the compaction behavior of distended materials in the partially compacted state (below P_s). The response of the foam in the partially compacted region is affected a great deal by its initial structure. The model handles this dynamic compaction, governed by the structure, by defining a suitable functional form for the variance of α in terms of state variables. The parameter α is the ratio of the density of the solid to the density of the foam at a given stress and internal energy. The functional form of α is empirically determined with certain boundary conditions. The principal conditions are that $\alpha = 1$ when the foam is fully compacted (at P_s), and that the transition of this state is continuous. The simple functional form used in this work was a Taylor's series expansion of α in terms of stress (P) up to the third order

$$\alpha = a_0 + a_1 P + a_2 P^2 + a_3 P^3 \qquad (1)$$

If the quadratic form is used, P_s and the initial distention ratio are sufficient conditions to evaluate a_0, a_1, and a_2. It will be shown for the graphitic carbons that the quadratic function gives adequate agreement between the experimental data and the model predictions. A cubic $P - \alpha$ relation was required to represent the amorphic materials in the partially compacted state, in which case a_3 had to be determined. The low-pressure data, which reflect the effect of the initial carbon structure, were used to evaluate a_3. Therefore, the $P - \alpha$ model requires as input the solid material equation of state, the stress (P_s) at which the foam compacts to a no void condition, the initial porosity of the foam and a functional relation between P and α.

In the high-pressure region (above P_s) of complete compaction, the structural details of the original structure are destroyed and the material is in a solid state. Techniques for calculating state points for a distended material compacted to a no void condition have been previously presented.[18,19] At these pressures (above P_s) the Rankine-Hugoniot relations were used in conjunction with the Mie-Gruneisen equation of state to define the compacted porous materials equation of state.[8] The resulting expressions make use of a known reference state of the associated solid material. This Hugoniot description for the fully compacted region and the $P - \alpha$ model for the partially compacted region are quite compatible because the $P - \alpha$ model reduces to the Hugoniot description at pressures above P_s.

As previously discussed, the equation of state of the solid form of carbon present in the distended material is required for the calculations. Accurately defining the solid equation of state to represent the carbons investigated is difficult due to the uncertainty in the materials' structure. The material used to represent the solid in the calculations was pyrolytic graphite. It was felt that 2.2 g/cc pyrolytic graphite would adequately represent the solid for the two graphitic materials and could possibly suffice for the amorphic group also.[20–22]‡ The choice of pyrolytic graphite was based on the fact that it is graphitic and has a density very near that of crystalline graphite (2.25 g/cc).

The Hugoniot data and calculated loading curves for the two materials considered graphitic are shown in Fig. 5 along

Table 4 Spallation results

Material	Impact velocity for spall, ft/sec	Pulse duration, μsec	Spall stress, kilobars
C/C-1	60 ± 10	0.65 & 2.9	0.38
C/C-3	50 ± 10	2.7	0.36
C/C-4 (staked)	115 ± 10	2.9	0.73
PCF-CVD-U	140 ± 7	4.2	1.00
PCF-CVD-G	190 ± 10	11.0	0.53

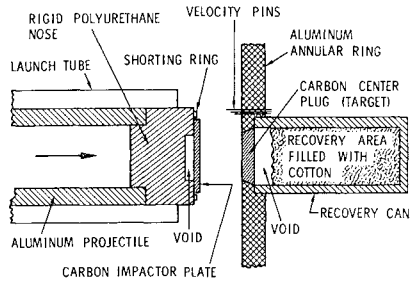

Fig. 4 Experimental configuration for spall tests.

‡ The pyrolytic graphite equation of state used in the model was the linear Hugoniot relation in the shock velocity-particle velocity plane. This relation, $U_s = 3.9 + 2.2\,u_p$, was obtained by combining the data from Refs. 20, 21, and 22 and making a least squares fit over the particle velocity range of interest ($0 < u_p < 1.3$). The value of 1.0 for γ was used.

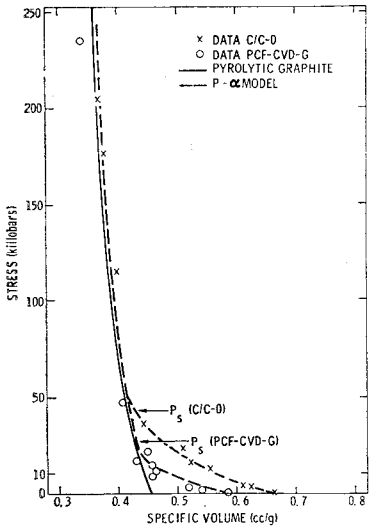

Fig. 5 Comparison of $P - \alpha$ model to Hugoniot data for C/C-O and PCF-CVD-G.

with the pyrolytic graphite Hugoniot. The offset between the pyrolytic graphite Hugoniot and the calculated response above P_s is due to the larger internal energy change encountered in compacting the foam. The calculated curves reproduce the data quite well. The quadratic $P - \alpha$ relation was used to represent the partially compacted region for these graphitic materials, and relatively low values of P_s were evident.

The predicted Hugoniots and experimental data for the amorphous carbons are presented in Figs. 6 and 7. Again the calculated curves and experimental data are in close proximity. A quadratic $P - \alpha$ function would not adequately represent the amorphous carbons. The cubic $P - \alpha$ form was used in conjunction with high values of P_s to obtain the agreement. This is believed to be an indication of the initial structural difference between the graphitic and amorphic materials. The parameters used in calculating the loading paths for the porous carbons are listed in Table 6.

Another experimentally observed difference between the graphitic and amorphic carbons was the transmitted shock wave profile in the lower stress region. The wave profiles in the graphitic materials gave no indication of a precursor and transmitted the shock as a single wave over the entire pressure range investigated. However, there was a low-amplitude precursor evident in the transmitted wave profiles for the amorphous materials. The precursor was not a typical elastic wave but rather was a ramp preceding the main shock with an amplitude of approximately 1.0 to 2.0 kbars. At stresses in the range of 45–65 kbars, the precursors

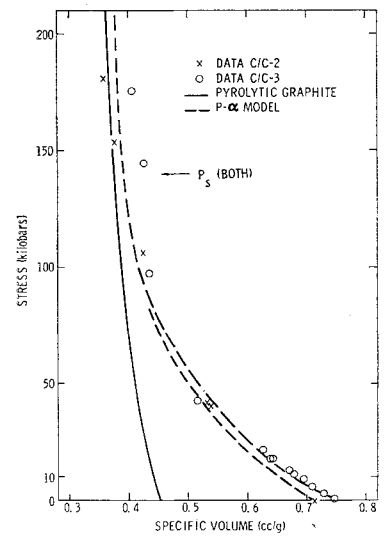

Fig. 6 Comparison of $P - \alpha$ model to Hugoniot data for C/C-2 and C/C-3.

Table 5 Attenuation data[a]

Target thickness, mm	Free surface velocity, mm/μsec
2.36	0.398
2.41	0.391
2.41	0.586
4.88	0.259
4.90	0.247
7.54	0.185
7.52	0.153
10.16	0.186
10.16	0.125

[a] Target material: C/C-1, impactor material: 0.010 in. mylar, and impact velocity: 1.083 mm/μsec.

were overtaken by the main shock and only a single wave was transmitted above these stresses. The shape of the precursor waves indicates a negative curvature of the stress-strain curves in the yield region for the amorphous carbons.

The effect of staking the C/C-1 filament material was evaluated using C/C-4. Both the C/C-1 and C/C-4 were produced in the same manner except for adding filaments in the third direction in C/C-4. There was no difference, within experimental error, in the Hugoniot data for the two materials as seen in Fig. 7.

Unloading Behavior

The shock mitigation effectiveness of a porous material is related directly to the hysteresis in its loading-unloading path, which represents the amount of energy dissipated during the cycle.[23] The attenuation of a shock pulse of finite duration propagating through a porous material is governed primarily by relief waves overtaking the initial shock front. The unloading paths for a material define the velocities of propagation and shapes of these relief waves. In shock wave calculations, the degree of attenuation in a porous material can be drastically altered depending on the unloading path assumed. Two possible unloading paths which represent the limits of possible material behavior have been considered. The first, designated "Unloading Path 1" assumes an unloading characteristic of the solid, thereby introducing the maximum possible hysteresis in the loading cycle. The second, designated "Unloading Path 2" is representative of a material which returns to its original volume after unloading. The effect of using these two descriptions to define the unloading behavior of C/C-1 in the partially compacted region can be seen in Fig. 8. This figure contains the attenuation data from exploding foil experiments for C/C-1 plotted as free surface velocity vs target thickness for constant impact conditions.[15] The data show a marked decrease in free surface velocity with distance of propagation. The two calculated attenuation curves were determined by treating the entire problem of initial impact, compressive shock wave propagation and subsequent unloading in the mylar impactor and carbon target. The impactor and target dimensions and the impact velocity used in the calculations were the same as those in the experiment. The equation of state data from this study were used to describe the carbons. The mylar was characterized as hydrodynamic using existing equation of state information.[24] Only the assumed unloading path was changed in the numerical computer calculations that generated these two attenuation curves.[25] The calculated curves do not agree with the experimental results. This strongly indicates that the true unloading path does not compare to either extreme.

Figure 8 illustrates the importance of accurately defining the actual unloading behavior of partially compacted porous carbons in order to ascertain their effectiveness as shock mitigators. One velocity interferometer experiment designed to record the unloading wave profile was performed on

Table 6 Inputs for $P - \alpha$ model computations

Solid taken as pyrolytic graphite with $v_0 = 0.454$; $c_0 = 3.9$ mm/μsec; $s = 2.2$

Material	Degree of $P - \alpha$ fit	a_3, $\Delta\alpha$/kbar	v_0, cc/g	P_s, kbar	γ^a
C/C-0	Quadratic	...	0.662	50	1
PCF-CVD-G	Quadratic	...	0.585	24	1
C/C-1, −4	Cubic	−0.014	0.714	120	1
C/C-2	Cubic	−0.010	0.725	140	1
C/C-3	Cubic	−0.010	0.746	140	1
PCF-CVD-U	Cubic	−0.012	0.568	60	1

[a] The calculated loading curves were relatively insensitive to the value of γ used.

C/C-1. The measured unloading path was not in agreement with either of the assumed unloading paths used in the previous attenuation calculations but was between these two extremes. This type of unloading behavior has also been observed by Lysne on a 1.37 g/cc carbon.[26] Using the unloading wave data for C/C-1 and a finite difference code WONDY III which incorporates the $P - \alpha$ model, another attenuation curve was calculated to compare with the experimental results.[27] The calculated free surface velocity points are also shown in Fig. 8 and are referred to as WONDY calculations. Good agreement is shown between the calculated points and the attenuation data.

Based on limited evidence, it appears that for stresses above P_s, the distended carbons unload from shock states along paths characteristic of solid pyrolytic graphite. This is indicated by free surface velocity measurements made on C/C-3 above P_s. The (σ,u_p) state arrived at by an impedance match solution for these experiments and the state obtained by assuming solid unloading through the measured u_{fs} are in close agreement. Also free surface velocity measurements on C/C-3 made below P_s show a trend toward the solid unloading path as pressure increases.

Spallation Results

The spallation stress or dynamic tensile strength in one dimensional strain is an important material property in the characterization of the distended carbons. The spall strengths of the five materials tested were found to be 1 kbar or less. The materials in the order of increasing spall strengths are the filament system (C/C-1 and C/C-3 with 0.38 and 0.36 kbar, respectively), the staked filament system (C/C-4 with 0.73 kbar), and the carbon felt-carbon vapor deposited system (PCF-CVD-U and PCF-CVD-G with 1.0 and 0.5 kbar, respectively). As was expected, the staking in the third direction in C/C-4 increased the dynamic interlaminar tensile strength of the filament system. The staking increased the spall strength by approximately a factor of two. The graphitization of the PCF-CVD material decreased its spall strength from 1.0 to 0.5 kbar.

Conclusions

1) The Hugoniots for the seven distended carbons studied can be suitably fitted in the partially compacted region using the $P - \alpha$ model and pyrolytic graphite to represent the solid material.

2) The initial structure or graphite content has a significant effect on the dynamic response of the distended carbons in the partially compacted region.

3) The transmitted wave profiles in the graphitic systems are single shocks while the amorphous materials support a ramp shaped precursor with an amplitude of 1.0 to 2.0 kbars. The precursor is overdriven by the main shock at stresses between 45 to 65 kbars.

4) The unloading behavior of these distended materials in the partially compacted region is not adequately described by either of the two limiting unloading approximations but is somewhere between these limits. In the region above P_s, the materials appear to unload along a path characteristic of solid pyrolytic graphite.

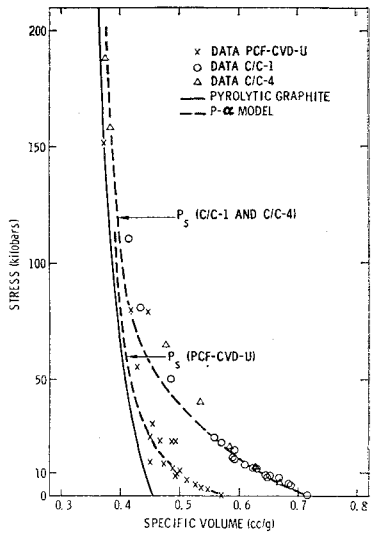

Fig. 7 Comparison of $P - \alpha$ model to Hugoniot data for C/C-1, C/C-4, and PCF-CVD-U.

5) The spallation strengths for the carbons tested were all less than 1.0 kbar with the PCF-CVD-U material being the strongest. Graphitizing the PCF-CVD-U decreased the spall strength from 1.0 to 0.5 kbar. Staking the filament material in the third direction increased its spall level by approximately a factor of two.

Appendix: Equation of State of Crushable Distended Materials

The dynamic compression data in the partially compacted region were fitted to the $P - \alpha$ description of the equation of state of crushable porous materials proposed by Herrmann.[17] Thermodynamic equilibrium is assumed. The parameter α relates the instantaneous density of the foam at a given pressure and internal energy to the density of the solid for the same conditions:

$$\alpha\rho_F = \rho_s \qquad \text{(A1)}$$

The symbols and constants for the derivation are defined in the list of symbols.

The Rankine-Hugoniot equation which relates the energy of the shocked state to the pressure, volume, and prior state of the material is used to calculate the change in internal

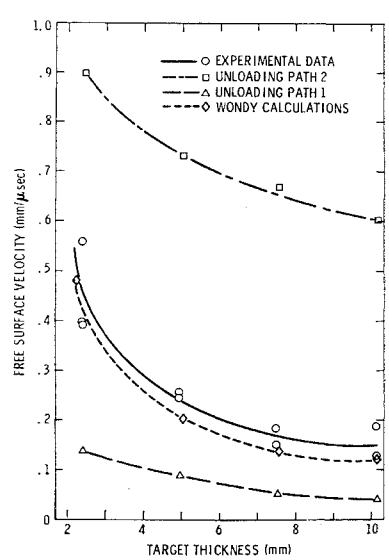

Fig. 8 Experimental data and calculated attenuation curves for C/C-1.

energy,

$$\mathcal{E}_F = \mathcal{E}_{F0} + \frac{(P + P_0)}{2}\left(\frac{1}{\rho_{F0}} - \frac{1}{\rho_F}\right) \tag{A2}$$

where the subscripts 0 indicate the initial unstressed conditions.

Once the change in internal energy is established, the density of the solid is obtained from the Gruneisen equation of state,

$$P = P_r + \gamma\rho_s(\mathcal{E} - \mathcal{E}_r) \tag{A3}$$

The product $\gamma\rho_s$ was held constant, and a linear $U_s - u_p$ Hugoniot relation was used for the reference states $(P_r,\mathcal{E}_r)$

$$U_s = c_0 + su_p \tag{A4}$$

The constants for pyrolytic graphite used were $c_0 = 3.9$ mm/μsec, $s = 2.2$, and $\gamma_0 = 1.0$. The resulting expressions for P_r and ϵ_r are

$$P_r = \frac{\rho_{s0}c_0^2(1 - \rho_{s0}/\rho s)}{[1 - s(1 - \rho_{s0}/\rho_s)]^2}$$
$$\mathcal{E}_r = \frac{P_r}{2}\left\{\frac{1}{\rho_{s0}} - \frac{1}{\rho_s}\right\} + \mathcal{E}_{s0} \tag{A5}$$

The final relation between P, α, and ρ_F or ρ_s is obtained by substituting Eqs. (A1), (A2), and (A5) into (A3)

$$P = \frac{\dfrac{\rho_{s0}c_0^2(1 - \rho_{s0}/\rho_s)}{[1 - s(1 - \rho_{s0}/\rho_s)]^2}\left[1 - \dfrac{\gamma_0}{2}\left(1 - \dfrac{\rho_{s0}}{\rho_s}\right)\right]}{\left[1 - \dfrac{\gamma_0}{2}\left(\alpha_0 - \dfrac{\rho_{s0}\alpha}{\rho_s}\right)\right]} \tag{A6}$$

$$P = \frac{\dfrac{\rho_{s0}c_0^2(1 - \rho_{s0}/\alpha_{0F})}{[1 - s(1 - \rho_{s0}/\alpha\rho_F)]^2}\left[1 - \dfrac{\gamma_0}{2}\left(1 - \dfrac{\rho_{s0}}{\alpha\rho_F}\right)\right]}{\left[1 - \dfrac{\gamma_0}{2}\left(\alpha_0 - \dfrac{\rho_{s0}}{\rho_F}\right)\right]} \tag{A7}$$

where $\gamma\rho_s = \gamma_0\rho_{s0}$ and $\mathcal{E}_{F0} = \mathcal{E}_{s0}$

For pressures above P_s, i.e., $\alpha = 1$, Eq. (A7) reduces to the form previously presented.[18,19]

References

[1] Mantell, C. L., *Carbon and Graphite Handbook*, Interscience, New York, 1968.

[2] Chalykh, Ye. F., *Technology of Carbon-Graphite Materials*, Literary Po Chernoy i Tsvetnoy Metalurgii, Moscow, 1963.

[3] Pierson, H. O. and Smatana, J. F., "Development and Properties of Pyrolytic Carbon Felt Composites," *Proceedings of the 14th National Symposium of the Society of Aerospace Material and Process Engineers*, Nov. 1968.

[4] Barker, L. M. and Hollenbach, R. E., "System for Measuring the Dynamic Properties of Materials," *The Review of Scientific Instruments*, Vol. 35, No. 6, 1964, pp. 742–746.

[5] Butcher, B. M. and Canon, J. R., "Influence of Work-Hardening on the Dynamic Stress-Strain Curves of 4340 Steel," *AIAA Journal*, Vol. 2, No. 12, Dec. 1964, pp. 2174–2179.

[6] Graham, R. A., Neilson, F. W., and Benedick, W. B., "Piezoelectric Current From Shock-Loaded Quartz—A Submicrosecond Stress Gauge," *Journal of Applied Physics*, Vol. 36, No. 4, 1965, pp. 1775–1783.

[7] Lee, L. M., "Dynamic Compaction of Distended Isotropic Boron Nitride," SC-RR-68-2, March 1968, Sandia Laboratories, Albuquerque, N.Mex.

[8] Rice, M. H., McQueen, R. G., and Walsh, J. M., "Compression of Solids by Strong Shock Waves," *Solid State Physics*, edited by F. Seitz and D. Turnbull, Vol. 6, Academic Press, New York, 1958, pp. 1–63.

[9] Van Thiel, M., Kusubov, A. S., and Mitchell, A. C., "Compendium of Shock Wave Data," UCRL 50108, Vol. II, Lawrence Radiation Laboratory, Livermore, Calif.

[10] Boade, R. R., "Shock Compression of Foamed Graphite," *Journal of Applied Physics*, Vol. 39, No. 3, 1968, pp. 1609–1617.

[11] Barker, L. M., "Fine Structure of Compressive and Release Wave Shapes in Aluminum Measured by the Velocity Interferometer Technique," *Symposium on High Pressure, I.U.T.A.M., Paris, France*, Gordon and Bead, New York, 1968, pp. 483–505.

[12] Barker, L. M., private communication.

[13] Guess, T. R. and Lee, L. M., "Spall Strengths of Five Carbon Materials," SC-DR-68-604, Oct. 1968, Sandia Laboratories, Albuquerque, N.Mex.

[14] Butcher, B. M. et al., "Influence of Stress History on Time-Dependent Spall in Metals," *AIAA Journal*, Vol. 2, No. 6, June 1964, pp. 977–990.

[15] Davies, F. W. and Penning, J. R., "Free Surface Velocity Measurements of Some Ablative Materials," SC-CR-68-3633, Sandia Laboratories, Albuquerque, N.Mex.

[16] Keller, D. V. and Penning, J. R., Jr., "Exploding Foils—The Production of Plane Shock Waves and the Acceleration of Thin Plates," *Exploding Wires*, Vol. 2, Plenum Press, New York, 1962.

[17] Herrmann, W., "Equation of State of Crushable Distended Materials," SC-RR-66-2678, March 1968, Sandia Laboratories, Albuquerque, N.Mex.

[18] Krupnikov, A. K., Brazhnik, M. I., and Krupnikova, V. P., "Shock Compression of Porous Tungsten," *Soviet Physics JETP*, Vol. 15, Sept. 1962, pp. 470–476.

[19] Kormer, S. B. et al., "Dynamic Compression of Porous Metals and the Equation of State with Variable Specific Heat at High Temperatures," *Soviet Physics JETP*, Vol. 15, Sept. 1962, pp. 477–488.

[20] Doran, D. G., "Hugoniot Equation of State of Pyrolytic Graphite to 300 kbars," *Journal of Applied Physics*, Vol. 34, No. 4, 1963, pp. 844–851.

[21] Coleburn, N. L., "Compressibility of Pyrolytic Graphite," *The Journal of Chemical Physics*, Vol. 40, No. 1, 1964, pp. 71–77.

[22] McQueen, R. G. and Marsh, S. P., "Hugoniots of Graphiques of Various Initial Densities and the Equation of State of Carbon," *Symposium on High Pressure, I.U.T.A.M., Paris, France*, Gordon and Bead, New York, 1968, pp. 207–216.

[23] Herrmann, W., "Basic Response Phenomenology and Anayltical Techniques," SC-R-68-1784, Aug. 1968, Sandia Laboratories, Albuquerque, N.Mex.

[24] Penning, J. R. and Davies, F. W., "Hugoniot Equation of State of Mylar," D2-125304-1, July 1968, Boeing Company, Seattle, Wash.

[25] Barker, L. M., "SWAP-7: A Stress-Wave Analyzing Program," SC-DR-67-143, April 1967, Sandia Laboratories, Albuquerque, N.Mex.

[26] Lysne, P. C., "Low Stress Shock and Release Wave Behavior of Porous Carbon," *Journal of Applied Physics*, Vol. 41, No. 1, 1970, pp. 351–360.

[27] Herrmann, W., "On the Elastic Compression of Crushable Distended Materials," SC-DR-68-321, June 1968, Sandia Laboratories, Albuquerque, N.Mex.